Self-Wound Composite Nanomembranes as Electrode Materials for Lithium Ion Batteries

By *Heng-Xing Ji, Xing-Long Wu, Li-Zhen Fan, Cornelia Krien, Irina Fiering, Yu-Guo Guo,* Yongfeng Mei,** and *Oliver G. Schmidt*

Bending and rolling is commonly employed in nature to release strain in films to maintain structure stability. Recently, rolled-up nanotechnology has proven to be an intriguing approach on the micro-/nanoscale for various promising future applications and concepts.[1–5] Nanomembranes composed of various functional stacks can self wind (or roll up) into micro/nanotubes upon detaching from a holding substrate by releasing intrinsic differential strain. The deposition and process methods for nanomembranes are compatible to industrial-level technologies like e-beam evaporation, sputtering deposition and atomic layer deposition, etc., which are demanded by advanced materials used for applications. Moreover, the intrinsic strain accommodated in multi-layer nanomembranes is efficiently released by self winding and thus offers a minimization of the system energy.[6] Such tubular and strain-relaxed structures are liable to improve the materials tolerance against stress cracking and are therefore promising candidates for increasing the stability of energy storage devices such as lithium ion batteries.

Lithium ion batteries are attractive for applications ranging from electric vehicles to microchips.[7–10] One of the big challenges is strain accommodation during electrode lithiation, which would prevent the electrodes in batteries from being pulverized which causes capacity fading.[10–12] For example, transition-metal oxides and lithium alloys are attractive anode materials owing to their high theoretical charge capacity, which is several times larger than existing graphite anodes.[13–16] Nevertheless, large volume changes (100% – 400%) of these electrodes during Li uptake/release cycling generate high strains and the electrodes tend to pulverize. Consequently, the battery capacity fades because of the electrode materials losing electron conduction.[17,18] One of the most promising approaches to enhance the cycling performance is the use of nanocomposites. For instance, nanostructures can increase the tolerance towards stress cracking, and nanocoating (by e.g., carbon) can increase the stability of the solid electrolyte interphase (SEI).[19–25] One of the optimized nanostructure designs is composed of two-dimensional nanowire arrays which are directly grown on current collectors. This concept was realized by both fabricating silicon nanowires via chemical vapor deposition and constructing metal oxides/carbon coaxial nanowire arrays by template assistance.[26–29] The idea to use three-dimensional mesoporous structures was also introduced, and proved by using mesoporous carbon as a stable and conductive framework to enhance the cycling performance of electrode materials.[30,31] However, the synthesis of nanocomposites is complicated; and the interface and the chemical distributions in such nanocomposite are hardly homogeneous.

Here, we apply rolled-up nanotechnology to produce composite micro/nanohierarchical materials for lithium ion batteries. As shown in **Figure 1a**, the composite nanomembranes can consist of materials with high capacity (e.g., Si, Sn, RuO_2, etc.) to serve as an active layer, and materials with high stability and electrical conductivity (e.g., carbon) to act as a supporting layer. Thus, the active layer mainly offers the lithium storage while the supporting layer maintains the structural integrity and provides quick electron transport. The thickness of the layers is readily controlled on the nanometer-scale, and the interface between different layers is homogenous ensuring electron and lithium ion transfer. In addition, the composite nanomembranes can consist of various materials including oxides, metals and nonmetals, which can meet different demands for the electrodes.[32,33] When removing the sacrificial layer (here photoresist), the composite nanomembranes automatically peel off from the substrate, break into micrometer-sized pieces and self-wind into microscale tubular rolls (Video 1, Supporting Information). The self-wound nanomembranes (SWNMs) build up a mixed electron/ion conductive network as the supporting layer serves as a continuous transport pathway for electrons, and the hollow nature of the SWNMs provide fast transport channels for Li^+. The hierarchical mixed conducting network has been proved to be a practical electrode design to improve the reaction kinetics of lithium ion batteries.[34,35] Moreover, the intrinsic strain of the SWNMs relaxes to a minimal level by rolling so as to improve the tolerance to stress cracking induced by volume expansion during Li^+ uptake.

[*] Dr. H. X. Ji, C. Krien, I. Fiering, Dr. Y. F. Mei, Prof. O. G. Schmidt
Institute for Integrative Nanosciences, IFW Dresden
Helmholtzstrasse 20, Dresden D-01069 (Germany)
E-mail: yongfeng.mei@gmail.com
Prof. O. G. Schmidt
Material Systems for Nanoelectronics
Chemnitz University of Technology
Reichenhainer Str. 70, Chemnitz D-09107 (Germany)
X. L. Wu, Prof. Y. G. Guo
Key Laboratory of Molecular Nanostructure and Nanotechnology and Beijing National, Laboratory for Molecular Sciences (BNLMS)
Center for Molecular Sciences
Institute of Chemistry, Chinese Academy of Sciences (CAS)
Beijing 100190 (China)
E-mail: ygguo@iccas.ac.cn
Prof L. Z. Fan
School of Materials Science and Engineering
University of Science and Technology Beijing
Beijing 100083 (China)
Prof. Y. F. Mei,
Department of Materials Science, Fudan University
Handan Road 220, 200433 Shanghai (China)

DOI: 10.1002/adma.201001422

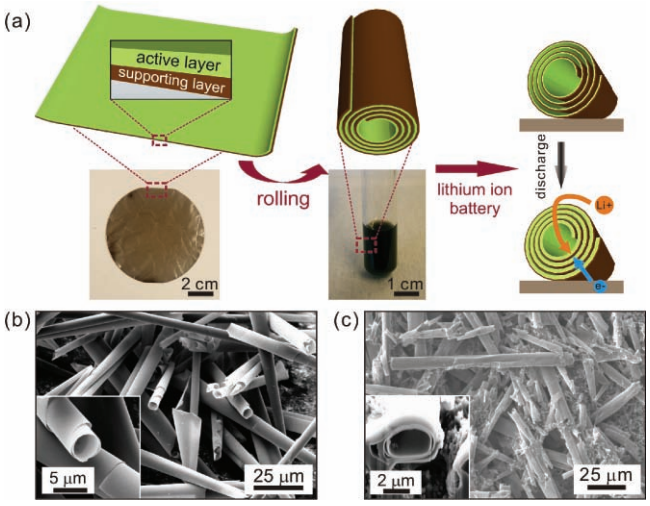

Figure 1. (a) Schematic illustration of the rolled-up process. The photo shows the composite nanomembrane (50 nm RuO_2/15 nm Carbon) on a 3 inch wafer with photoresist as a sacrificial layer, and the SWNMs suspension in acetone. (b), (c) SEM images of the SWNMs nanomembranes before (b) and after (c) mixing with PVDF binder. The insets show a detailed structure of the open ends.

Our proof-of-concept studies are based on ruthenium dioxide/carbon (RuO_2/C) composite nanomembranes, while they are by no means limited to these materials. The RuO_2 is used as the active layer owing to its ability to reversibly store lithium by a conversion reaction.[36] RuO_2 can achieve a favorable combination of high capacity and high coulombic efficiency compared to other materials.[37–39] However, a RuO_2/Li half-cell could only operate reversibly for a few cycles because of large volume expansion (100%) during cycling.[37–39] Carbon is employed to serve as the supporting layer because of its high stability as an anode material in lithium ion batteries and its reasonable electrical conductivity for charge separation.[18,19] The composite nanomembranes incorporating a 50 nm RuO_2 layer and a 15 nm carbon layer were deposited by RF-sputtering on an aluminum foil (Figure 1a). The chemical composition of the composite nanomembranes was measured by X-ray photoelectron spectroscopy and Raman spectroscopy (Figure S1 and S2, Supporting Information) and confirms the Ru/O stoichiometry of RuO_2 as well as the formation of RuO_2/C composites, respectively. The RuO_2/C composite nanomembranes were released from the sacrificial layer by immersing the wafer into acetone to prepare SWNMs. The yield of the SWNMs is around 95% as shown in the low magnification scanning electron microscopy (SEM) image (Figure S3). The detailed morphology of the freshly prepared SWNMs is shown in Figure 1b, in which each SWNM presents an open end and a smooth wall that originates from the flat morphology of the initially deposited thin film. The diameter of the SWNMs is around 5 μm as shown in both the inset of Figure 1b and Figure S3. Then, the SWNMs were mixed with acetylene black, polyvinylidene fluoride (PVDF) at a weight ratio of 70:20:10 to prepare work electrodes for battery cycling. The morphology of the work electrode is shown in Figure 1c consisting of one-dimensional microstructures with open ends. One SWNM in the electrode was cut by focus ion beam (FIB) to reveal the profile of the structure, which has a hollow inside and layered windings as seen in the inset of Figure 1c. This result proves that the SWNMs are strong enough to withstand the casting and pressing process necessary for battery assembly.

The electrochemical properties of the RuO_2/C SWNMs with respect to Li insertion/extraction were investigated, and those of a commercial RuO_2 powder (Aldrich) were also studied for comparison. The galvanostatic discharge/charge voltage profiles at C/16 rate (means a fully discharge in 16 hours) are depicted in **Figure 2a**. The first discharge curves of both the RuO_2 powder and the RuO_2/C SWNMs show three distinct regions (a, b, and c), which correspond to different reaction stages:[37]

$$\text{region a (plateau around 2.1V)} : RuO_2 + Li^+ + e^- \rightarrow LiRuO_2$$

$$\text{region b (plateau around 0.9V)} : LiRuO_2 + 3Li^+ + 3e^- \rightarrow 2Li_2O + R$$

$$\text{region c (slope after 0.9V)} : Li_2O + Ru + xLi^+ + xe^- \rightarrow Li_2O : xLi : Ru$$

$$yLi^+ + ye^- + \text{electrolyte} \rightarrow SEI(yLi)$$

That means Region c corresponds to a surface charge-transfer lithium storage process in which the lithium ions can

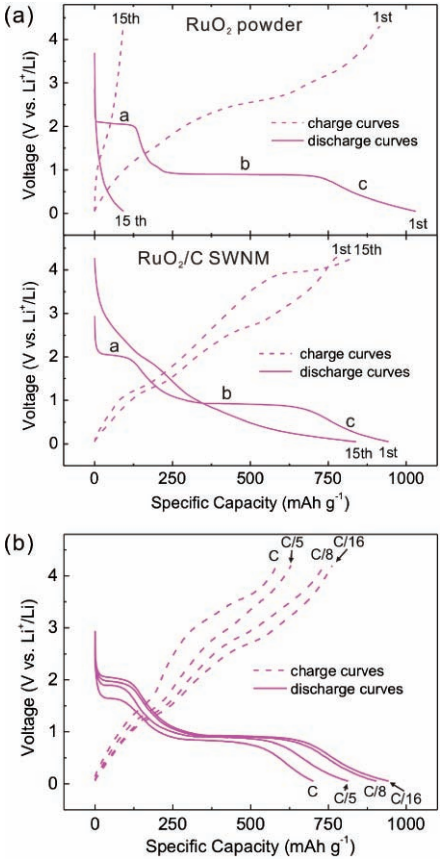

Figure 2. (a) Galvanostatic discharge/charge curves of the RuO_2 powder and the RuO_2/C SWNMs at the C/16 rate between 0.05 V and 4.3 V. (b) Galvanostatic discharge/charge curves of the RuO_2/C SWNMs at different rates.

be further stored at the boundary via charge separation between the Li_2O and metallic Ru interface.[37] This hypothesis is confirmed by the fact that the specific discharge capacities of both the RuO_2 powder and the RuO_2/C SWNMs reach a high value around 1000 mA h g^{-1} which is larger than the theoretical value of 806 mA h g^{-1}.[40] In addition, the formation of the SEI film could partly contribute to the discharge capacity as the SEI film mainly forms below 0.8 V during discharge.[37,39] The coulombic efficiency in the first cycle of the RuO_2 powder and the RuO_2/C SWNMs are 88% and 83%, respectively, which is higher than that of most transition-metal oxides. This is a typical feature of nanocrystalline RuO_2 for Li^+ insertion which was first reported by J. Maier et al.[37–39] However, the discharge capacity of the RuO_2 powder is reduced to 90 mA h g^{-1} in the fifteenth discharge cycle, suggesting that the RuO_2 powder/Li half-cell has failed, which agrees with results previously reported.[37] On the other hand, the fifteenth discharge/charge curves for the RuO_2/C SWNMs still show a feature of RuO_2, and reach a discharge capacity of 830 mA h g^{-1} and a coulombic efficiency of 99%, which implies enhanced lifetime and good reversibility of the RuO_2/C SWNMs. The SWNMs also show high specific capacity at higher discharge/charge rates. Figure 2b shows the discharge/charge curves measured at rates of C/16, C/8, C/5 and 1C. At 1C, the specific capacity of the SWNMs is still as high as 700 mA h g^{-1}.

The cycling performance of both the SWNMs and the RuO_2 powder at C/16 are shown in **Figure 3a**. The RuO_2 powder/Li half-cell fails within five cycles. The specific capacity of the RuO_2/C SWNMs decreases down to 600 mA h g^{-1} over the initial four cycles, but then increases gradually until in the eighteenth cycle a high value of 1000 mA h g^{-1} is reached, which is close to the initial specific capacity of the RuO_2/C SWNMs. To understand this specific feature of the performance, the coulombic efficiencies of the RuO_2/C SWNMs are depicted in Figure 3b. In the initial two cycles, the specific capacity of the RuO_2/C SWNMs fades and the coulombic efficiency is around 83%. However, the coulombic efficiencies rise to more than 100% from the third to fifth cycle when also the specific capacity increases. Considering together with the discharge/charge properties of SWNMs, the first discharge curve of the RuO_2/C SWNM (Figure 2a) reaches a specific capacity of 950 mA h g^{-1}, which is 92% of the RuO_2 powder (1030 mA h g^{-1}), suggesting that the Li^+ can access most parts of the RuO_2 in the SWNMs to form Li_2O and Ru. However, the first discharge induces a volume expansion of the active layer in the SWNMs, which may block the Li^+ transfer in the succeeding charging process. Therefore, part of the Li_2O is possibly left in the SWNMs together with RuO_2 after the first charge, consequently the capacity decreases and the coulombic efficiency is low in the first and the second cycles. After three cycles, the space between the layers of the SWNMs becomes larger. The Li_2O and Ru that formed in the initial cycles can now access the electrolyte solution to react back to Li^+ and RuO_2 from the fourth charge on. Consequently, the amount of the Li_2O and Ru for charging is larger than that formed at the end of the fourth discharging cycle, hence resulting in a high coulombic efficiency larger than 100%. In addition, besides the gradual penetration of electrolyte into the SWNMs' interior, the gradual decomposition of SEI could also contribute to the capacity increase upon cycling.[37] In the following cycles, the specific capacity of the RuO_2/C SWNMs approaches that at the initial cycle, indicating enhanced cycling performance and reversibility. It is worth to note that the specific capacity of most transition-metal oxides drops by more than 20% in the first cycle, and would not rise back due to pulverization and nonreversible reaction such as the formation of SEI film.[14] The cycling performance of the SWNMs is also superior to the poor performance of the RuO_2 powder that is caused by the conversion reaction.[37–39]

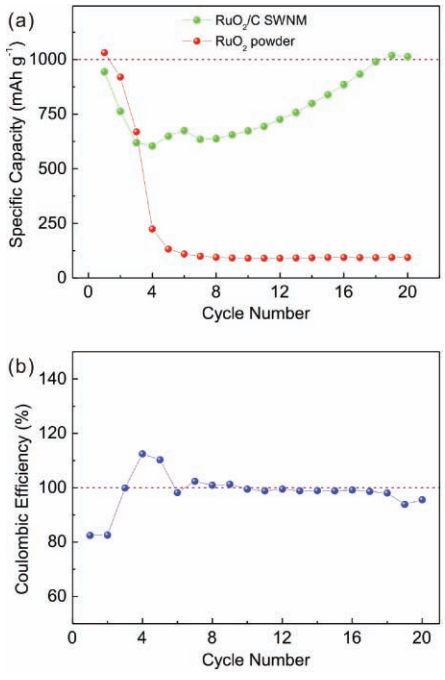

Figure 3. (a) Cycling performance of the RuO_2/C SWNMs and the RuO_2 powder at C/16. (b) Coulombic efficiency of the RuO_2/C SWNMs at different cycles.

To further understand the cycling performance, the morphology evolution of the RuO_2/C SWNMs at different cycling stages was studied. The SEM images of the RuO_2/C SWNMs at the initial state, after the first discharge at 0.05 V (vs. Li^+/Li) and after the first charge at 4.3 V (vs. Li^+/Li) are depicted in **Figure 4** (the cross sections of the SWNMs are shown in Figure S4 in the supporting information). At the initial state, the SWNM shows a smooth surface and a well-defined geometry due to the roll-up of the nanomembrane. After the first discharge the SWNMs has a rough surface which could be due to both the volume expansion induced by conversion reaction (region a, b, and c in Figure 2a) and the formation of an SEI film which mainly grows within region c when discharging.[39] However, after the first charge, the smooth surface and the rolling edge of the SWNM can be seen again, indicating a good SWNM structural integrity and a reversible decomposition of the SEI film as it decomposes in particular above 3.8 V on charge.[39] This result confirms that the specific capacity fade over the initial three cycles is mainly due to the Li_2O conversion and not because of SWNMs pulverization. Therefore, the RuO_2/C SWNMs maintains a high specific capacity and reversibility in the following cycles as well as superior cycling performance over that of the RuO_2 powder. Obviously,

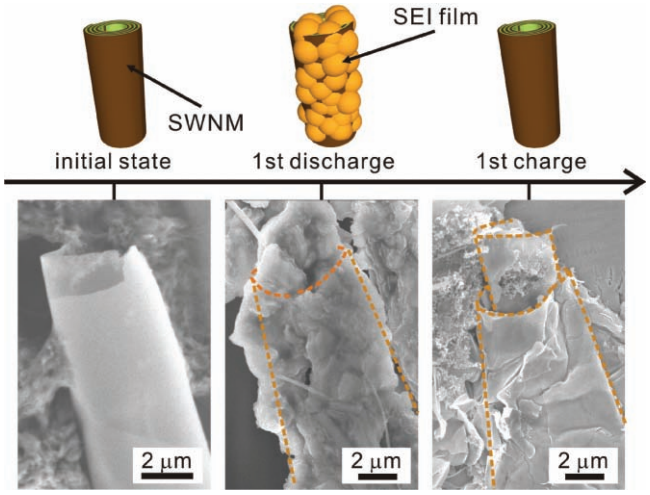

Figure 4. Morphology evolution of the SWNMs during Li uptake/release processes.

the new structure of the SWNM leads to several advantages. First, the relaxed strain, the tubular structure and the nanometer-thick active layer (RuO_2) of the SWNMs allows for enhanced tolerance to stress cracking. Second, the stable supporting layer (carbon) maintains the SWNMs structural integrity during the conversion reaction of the active layer which would break the homogeneity of the structure. Furthermore, the whole active layer adheres to the conductive supporting layer surface, which leads to large electron contact area and good adherence.

In addition, the synthesis procedure of the SWNMs is based on general film deposition techniques, which can be readily adapted to other interesting materials. Two attractive candidates are: (i) silicon, which possesses the highest theoretical capacity but suffers from poor cycling performance;[16,41] and (ii) $LiFePO_4$, which is a promising cathode material in electric vehicles, but its electron and Li^+ conduction needs still to be improved.[42,43] Furthermore, the thickness of both the active layer and the supporting layer can be tuned by changing the deposition time. The diameter of the SWNMs can easily be varied by the deposition parameters, such as the deposition power and pressure.[5] An optimized SWNMs structure is expected to deliver better cycling performance. Moreover, owing to the micrometer-size of the SWNMs, individual SWNM can be picked to study the interface change and ion diffusion effect on the Li^+ insertion/extraction in a certain area.[44]

In summary, we have demonstrated a new strategy to produce composite micro/nanohierarchical structures for lithium ion batteries. The enhanced cycling performance of lithium ion batteries based on self-wound nanomembranes as electrode materials benefits from several advantages including "elastic strain minimization", homogeneous distribution of the active material among the structure as well as the composite micro/nanohierarchical structure. This approach can easily be transferred to other materials that are available in 2D form by general thin film deposition techniques, and which meet various demands in lithium ion batteries. Furthermore, self-wound nanomembranes represent an interesting model system to study the interface effect and ion diffusion on the performance of lithium ion batteries with a flexible design in material compositions and microstructure.

Experimental Section

Synthesis: A photoresist (ARP 3510, Allresist) was used as a sacrificial layer by spin coating at 4500 rpm for 35 s before baking at 95 °C in an oven. Both RuO_2 and carbon nanomembranes were prepared by using RF-sputtering. 50 nm RuO_2 was deposited at 100 W, 5×10^{-3} mbar Ar/O_2 (4:1) with metallic Ru as a target. 15 nm carbon was deposited at 200 W, 7.5×10^{-4} mbar Ar with graphite as a target. After deposition, the sample was directly immersed into acetone. When the sacrificial layer dissolving, the RuO_2/C nanomembranes break into micrometer-sized pieces and self-wind into tubular rolls.

Material Characterization: The XPS measurements were carried out using a PHI 5600 CI (Physical Electronics) spectrometer. Mg Kα excitation (350 W) was used. The Raman spectroscopy was performed using InVia PL/Raman microscopes (Renishaw) with an excitation line at 442 nm. SEM (NVision 40 CrossBeam, Carl Zeiss) was used to investigate the morphology of the SWNMs.

Electrochemical Characterization: Electrochemical measurements were performed using two-electrode Swagelok-type cells assembled in an argon-filled glove box. For preparing the working electrodes, a mixture of RuO_2/C SWNMs or RuO_2 powder, Super-P acetylene black and poly(vinyl difluoride) (PVDF, Aldrich) at a weight ratio of 70:20:10, was pasted on pure Ti foil (99.6%, Goodfellow). Pure lithium foil was used as a counter electrode. A glass fiber (GF/D) from Whatman was used as separator. The electrolyte consisted of a solution of 1 M $LiPF_6$ in ethylene carbonate (EC)/dimethyl carbonate (DMC)/diethyl carbonate (DEC) (1:1:1, in wt%) obtained from Tianjin Jinniu Power Sources Material Co., Ltd. Galvanostatic cycling of the assembled cells was carried out using an Arbin BT2000 system in the voltage range of 0.05–4.3 V (vs. Li^+/Li). We used the total mass weight of the RuO_2/C SWNMs when calculating the specific capacity of the composite.

Supporting Information

Supporting Information is available from the Wiley Online Library or from the author.

Acknowledgements

We thank Stefan Baunack, Steffen Oswald, Christoph Deneke, Xianghua Kong and Elliot J. Smith for help. H.X.J. is grateful to the Alexander von Humboldt Foundation for fellowship support. Y.G. Guo thanks the National Science Foundation of China (50730005) for support. L.Z. Fan thanks NSF of China (50873015) for support. This work was financially supported by the Grants from the Volkswagen Foundation (I/84 072), a Multidisciplinary University Research Initiative (MURI) sponsored by the U. S. Air Force Office of Scientific Research (AFOSR) Grant No. FA9550–09-1–0550, and the German Research Foundation (DFG) within the International Research Training Group 1215. Y.F.M. also thanks for the support by the Visiting Scholar Foundation of the National Key Laboratory of Fundamental Science of Micro/Nano-Device and System Technology at Chongqing University.

Received: April 19, 2010
Published online: September 13, 2010

[1] O. G. Schmidt, K. Eberl, *Nature* **2001**, *410*, 168.
[2] M. H. Huang, C. Boone, M. Roberts, D. E. Savage, M. G. Lagally, N. Shaji, H. Qin, R. Blick, J. A. Nairn, F. Liu, *Adv. Mater.* **2005**, *17*, 2860.
[3] V. Luchnikov, O. Sydorenko, M. Stamm, *Adv. Mater.* **2005**, *17*, 1177.
[4] D. J. Bell, L. X. Dong, B. J. Nelson, M. Golling, L. Zhang, D. Grutzmacher, *Nano Lett.* **2006**, *6*, 725.

[5] Y. F. Mei, G. S. Huang, A. A. Solovev, E. B. Urena, I. Moench, F. Ding, T. Reindl, R. K. Y. Fu, P. K. Chu, O. G. Schmidt, *Adv. Mater.* **2008**, *20*, 4085.
[6] P. Cendula, S. Kiravittaya, Y. F. Mei, C. Deneke, O. G. Schmidt, *Phys. Rev. B* **2009**, *79*, 085429.
[7] J. Maier, *Nat. Mater.* **2005**, *4*, 805.
[8] M. Armand, J. M. Tarascon, *Nature* **2008**, *451*, 652.
[9] M. S. Whittingham, *Chem. Rev.* **2004**, *104*, 4271.
[10] J. M. Tarascon, M. Armand, *Nature* **2001**, *414*, 359.
[11] N. Meethong, H. Y. S. Huang, S. A. Speakman, W. C. Carter, Y. M. Chiang, *Adv. Funct. Mater.* **2007**, *17*, 1115.
[12] T. Ohzuku, A. Ueda, N. Yamamoto, *J. Electrochem. Soc.* **1995**, *142*, 1431.
[13] J. O. Besenhard, J. Yang, M. Winter, *J. Power Sources* **1997**, *68*, 87.
[14] P. Poizot, S. Laruelle, S. Grugeon, L. Dupont, J. M. Tarascon, *Nature* **2000**, *407*, 496.
[15] H. Li, L. H. Shi, Q. Wang, L. Q. Chen, X. J. Huang, *Solid State Ion.* **2002**, *148*, 247.
[16] U. Kasavajjula, C. S. Wang, A. J. Appleby, *J. Power Sources* **2007**, *163*, 1003.
[17] Y. S. Hu, Y. G. Guo, W. Sigle, S. Hore, P. Balaya, J. Maier, *Nat. Mater.* **2006**, *5*, 713.
[18] J. W. Long, B. Dunn, D. R. Rolison, H. S. White, *Chem. Rev.* **2004**, *104*, 4463.
[19] P. G. Bruce, B. Scrosati, J. M. Tarascon, *Angew. Chem. Int. Ed.* **2008**, *47*, 2930.
[20] Y. G. Guo, J. S. Hu, L. J. Wan, *Adv. Mater.* **2008**, *20*, 2878.
[21] D. R. Rolison, R. W. Long, J. C. Lytle, A. E. Fischer, C. P. Rhodes, T. M. McEvoy, M. E. Bourga, A. M. Lubers, *Chem. Soc. Rev.* **2009**, *38*, 226.
[22] B. Kang, G. Ceder, *Nature* **2009**, *458*, 190.
[23] Y. Wang, G. Z. Cao, *Adv. Mater.* **2008**, *20*, 2251.
[24] X. W. Lou, C. M. Li, L. A. Archer, *Adv. Mater.* **2009**, *21*, 2536.
[25] W. M. Zhang, J. S. Hu, Y. G. Guo, S. F. Zheng, L. S. Zhong, W. G. Song, L. J. Wan, *Adv. Mater.* **2008**, *20*, 1160.
[26] M. H. Park, M. G. Kim, J. Joo, K. Kim, J. Kim, S. Ahn, Y. Cui, J. Cho, *Nano Lett.* **2009**, *9*, 3844.
[27] A. L. M. Reddy, M. M. Shaijumon, S. R. Gowda, P. M. Ajayan, *Nano Lett.* **2009**, *9*, 1002.
[28] C. K. Chan, H. L. Peng, G. Liu, K. McIlwrath, X. F. Zhang, R. A. Huggins, Y. Cui, *Nat. Nanotechnol.* **2008**, *3*, 31.
[29] L. Taberna, S. Mitra, P. Poizot, P. Simon, J. M. Tarascon, *Nat. Mater.* **2006**, *5*, 567.
[30] X. L. Ji, K. T. Lee, L. F. Nazar, *Nat. Mater.* **2009**, *8*, 500.
[31] X. L. Wu, L. Y. Jiang, F. F. Cao, Y. G. Guo, L. J. Wan, *Adv. Mater.* **2009**, *21*, 2710.
[32] P. Birke, W. F. Chu, W. Weppner, *Solid State Ion.* **1996**, *93*, 1.
[33] N. J. Dudney, B. J. Neudecker, *Curr. Opin. Solid State Mat. Sci.* **1999**, *4*, 479.
[34] Y. S. Hu, Y. G. Guo, R. Dominko, M. Gaberscek, J. Jamnik, J. Maier, *Adv. Mater.* **2007**, *19*, 1963.
[35] Y. G. Guo, Y. S. Hu, W. Sigle, J. Maier, *Adv. Mater.* **2007**, *19*, 2087.
[36] M. Armand, F. Dalard, D. Deroo, C. Mouliom, *Solid State Ion.* **1985**, *15*, 205.
[37] P. Balaya, H. Li, L. Kienle, J. Maier, *Adv. Funct. Mater.* **2003**, *13*, 621.
[38] O. Delmer, P. Balaya, L. Kienle, J. Maier, *Adv. Mater.* **2008**, *20*, 501.
[39] E. Bekaert, P. Balaya, S. Murugavel, J. Maier, M. Menetrier, *Chem. Mater.* **2009**, *21*, 856.
[40] Y. F. Zhukovskii, P. Balaya, E. A. Kotomin, J. Maier, *Phys. Rev. Lett.* **2006**, *96*, 058302.
[41] B. Key, R. Bhattacharyya, M. Morcrette, V. Seznec, J. M. Tarascon, C. P. Grey, *J. Am. Chem. Soc.* **2009**, *131*, 9239.
[42] X. J. Zhu, L. B. Cheng, C. G. Wang, Z. P. Guo, P. Zhang, G. D. Du, H. K. Liu, *J. Phys. Chem. C* **2009**, *113*, 14518.
[43] S. Y. Chung, J. T. Bloking, Y. M. Chiang, *Nat. Mater.* **2002**, *1*, 123.
[44] H. X. Ji, Y. F. Mei, O. G. Schmidt, *Chem. Commun.* **2010**, *46*, 3881.